Table of Contents

List of Figures

Chapter 1

Glossary

EL Entrainment Layer

ML Mixed Layer

CBL Convective Boundary Layer

LES Large Eddy Simulation

FA Free Atmosphere

GCM General Circulation Model

DNS Direct Numerical Simulation

Ri Richardson Number, the bulk Richardson Number is $\frac{gh}{\overline{\theta}_{ML}}\frac{\Delta\theta}{w^{*2}}$, $\Delta\theta = \overline{\theta}(h_1) - \overline{\theta}(h_0)$

Chapter 2

Introduction

2.1 Motivation and Research Questions

The daytime convective atmospheric boundary layer (CBL) over land starts to grow at sunrise when the surface becomes warmer than the air above it. Coherent turbulent structures (thermals) begin to form and rise since their relative warmth causes them to be less dense and so buoyant. the temperature profile of the residual nigtime boundary layer is stable i.e. potential temperature (θ) increases with height. The thermals rise to their natural bouoyancy level overshoot and then overturn or recoil concurrently dragging down warm stable air from above which is subsequently mixed into the growing turbulent mixed layer (ML) (Stull 1988). This mixing at the top of the CBL is known as entrainment and the region over which it occurs, the entrainment layer (EL). CBL entrainment occurrs via distortion of buoyancy driven thermals by the buoyancy difference (jump) caused upon overshoot. These opposing buoyant forcings make for interesting dynamics.

CBL height (h) and the prediction thereof are important for calculating the concentration of any species and the sizes of the turbulent structures. In combination with the lifting condensation level knowledge of EL depth allows predictions pertaining to the formation of cumulous clouds. For example cloud cover increases as more thermals rise above their lifting con-

densation level. Parametrizations for both CBL growth and EL depth are required in mesoscale and general circulation models (GCMs). Furthermore it is an attractive goal to develop a robust set of scales for this region analogous to Monin-Obvukov Theory (Stull 1988, Traumner et al. 2011, Steyn et al. 1999, Nelson et al. 1989, Sorbjan 1996)

An effective, simplified conceptual model of the dry, shear-free CBL in the absence of large scale winds is represented in Figure 2.1. Turbulent mixing via upward moving thermals and corresponding cooler dowdraughts renders the average potential temperature $\overline{\theta}$ effectively constant within the ML. The average vertical turbulent heat flux ($\overline{w'\theta'}$) is positive and decreases as the thermals approach the CBL top. In the EL there is a mixture of turbulent thermals and relatively warmer stable air the proportion of the latter increasing with proximity to the free atmosphere (FA) above. In the EL $\overline{w'\theta'}$ becomes negative as the thermals which are now relatively cool impinge on the FA and turn downward pulling warmer air with them. The dimensionless parameter that represents the forcings under these conditions and is ubiquitous in the corresponding literature is the convective or buoyancy Richardson number (Ri = $frach\frac{g}{\overline{\theta}_{ML}}\Delta\theta w^{*2}$) (Deardorff et al. 1980, Stull 1988, Sullivan et al. 1998, Federovich et al. 2004, Brooks and Fowler 2012, Garcia and Mellado 2014). h is the CBL height and w^* is the convective velocity scale (Deardorff 1970) to be defined later.

The two principal external parameters in this simplified case, i.e. the dry, shear-free CBL in the absence of large scale winds, are the average vertical turbulent surace heat flux ($\overline{w'\theta'}_s$) and the upper lapse rate (γ) (Federovich et al. 2004,Sorbjan 1996). They have opposing effects, that is $\overline{w'\theta'}_s$ drives upward turbulent velocity (w'^+) and so CBL growth (w_e) wheras γ suppresses it. Conversely they both cause positive turbulent potential temperature perturbations (θ'^+) and so warming of the CBL. In the EL the thermals from the surface are now relatively cool. They turn downwards as they interact with the stable FA concurrently bringing down warmer stable are from above. Sullivan et al. 1998 demonstrated these tynamics by parti-

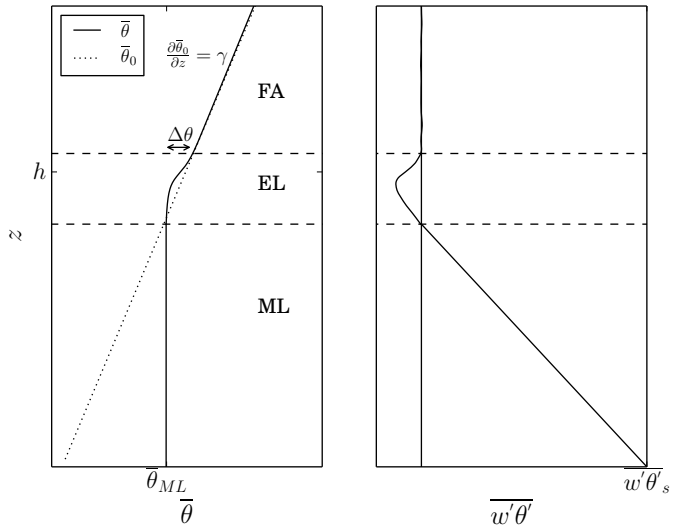

Figure 2.1

tioning $w^{'}\theta^{'}$ into four quadrants: upward moving warm ($w^{'+}\theta^{'+}$), downward moving warm ($w^{'-}\theta^{'+}$), upward moving cool ($w^{'+}\theta^{'-}$) and downward moving cool ($w^{'-}\theta^{'-}$). Sorbjan 1996 asserted and showed that in this region the potential temperature perturbations ($\theta^{'}$) are strongly influenced by γ whereas the turbulent vertical velocity peturbations ($w^{'}$) are almost independent thereof. Inspired by these two studies and to gain some insight into the dynamics of this idealized CBL I ask **Q1: How do the distrubutions of local CBL height, and $\theta^{'}w^{'}$ within the EL, vary with $\overline{w'\theta'}_s$ and γ?**

The relationship between scaled EL depth and Ri

$$\frac{\Delta h}{h} \propto Ri^{b} \tag{2.1}$$

has been explored and justified in measurement, laboratory, numerical and based studies. There is some disagreement with respect to its exact form, in part stemming from variation in defininition, but general its magnitude relative to h decreases with increasing Ri. Although referred in most rele-

vant studies to and relied upon in analytical models, the average potential temperature profile has not been used to define the EL(Deardorff et al. 1980, Nelson et al. 1989, Federovich et al. 2004, Boers 1989, Brooks and Fowler 2012). This leads me to ask **Q2: How can the EL limits be defined based on the $\overline{\theta}$ profile and what is the relationship of the resulting depth (Δh) to Ri?**

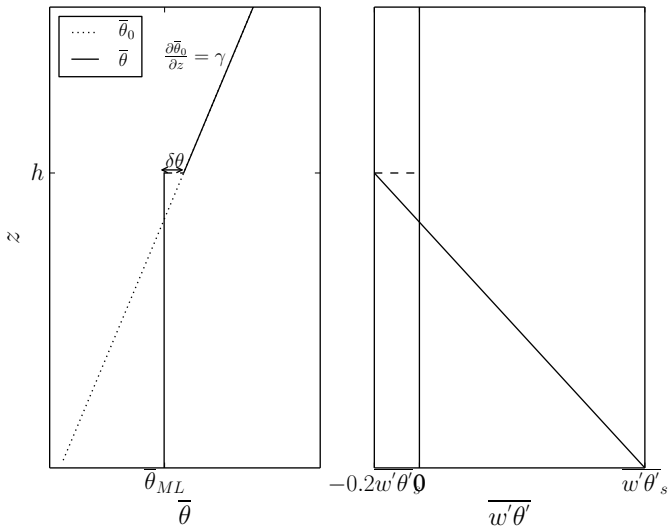

Figure 2.2

A further simplification to the dry, shear-free, CBL model without large scale velocities, is to regard the EL depth as infinitessimly small as in Figure 2.2. The relationship of the sca;ed, time rate of change of h (entrainment rate w_e), to Ri can be derived based on this model (Tennekes 1973, Deardorff 1979, Federovich et al. 2004)

$$\frac{w_e}{w^*} \propto Ri^a \tag{2.2}$$

.

This will be referred to as the entrainment relation. Although that there is

such a relationship is well esablished, discussion as to the power exponent of Ri is unresolved and results from studies justify values of both $-\frac{3}{2}$ and -1. See Traumner et al. 2011 for a summary and review. Turner 1986 explains this disparity in terms of entrainment mechanism such that the higher value occurrs when thermals recoil rather than overturn in response to a stronger θ jump (or inversion). Whereas Sullivan et al. (1998) notice a deviation from the lower power (-1) at lower Ri and attribute it to the effect of a the shape of $\overline{\theta}$ within a thicker EL. Both Federovich et al. (2004) and Garcia and Mellado (2014) show how the definition of the θ jump influences the time rate of change of Ri and so effects a. **Q3: How does defining the θ jump based on the vertical $\overline{\theta}$, i.e. accross the EL as in Figure 2.1 vs at the inversion (h) as in Figure 2.2, effect the entrainment relation, in particular a?**

2.2 Relevant Background

2.2.1 The Convective Boundary Layer (CBL)

The convective boundary layer over land starts to grow at rapidly at sunrise, peaking at midday. Convective turbulence and the dominant upward vertical motions then begin to subside as the surface cools. In the morning as the surface warms relative to the environment, instability causes thermals to develop and rise with buoyancy driven momentum. They are of uniform potential temperature (θ) and tracer concentration at their cores and entrain surrounding air laterally as they rise, as well as trapping and mixing in stable warm from above. (Stull [18], Crum et al. [3])

Under conditions of strong convection, buoyantly driven turbulence dominates and shear is insignificant (Fedorovich and Conzemius [10]). Thermals rise, overshoot their natural buoyancy level and overturn or recoil, trapping pockets (or wisps) of warm stable air which then becomes turbulently mixed. This overshoot and subsequent entrainment of the warmer air from

aloft augments the warming caused by the surface heat flux and results in a temperature jump ($\Delta\theta$). A potential temperature (θ) inversion may also be imposed and strengthened for example by subsidence.

Lidar images show the overall structure of the convective boundary layer (CBL) with the rising thermals, impinging on the air above. (Crum et al. [3], Traumner et al. [21]) This has been effectively modelled using large eddy simulation (LES) by Schmidt and Schumann in [13]. They used horizontal slices of potential temperature and vertical velocity perturbations ($\theta^{'}$, $w^{'}$) at various vertical levels to show how the thermals form, merge and impinge at the CBL top with concurrent peripheral downward motions. The latter is supported in the visualizations of Sullivan et al. in [19]. Vertical cross sections within the EL show relatively cooler thermal plumes and trapped warmer air as well as the closely associated upward motion of cooler air and downward motion of warmer air.

On average these convective turbulent structures create a mixed layer (ML) with eddy scales cascading from approximately the CBL height (h) to molecular diffusion according to the Kolmagorav power law. Here θ is close to uniform and $\overline{w^{'}\theta^{'}}$ is positive and decreasing. Warming is from both the surface heat flux ($\overline{w^{'}\theta^{'}}_s$) and the flux of entrained stable air at the inversion ($\overline{w^{'}\theta^{'}}_h$). ML turbulence is dominated by warm updraughts and cool downdraughts. With proximity to the top the updraughts become relatively cool and warmer air from above is drawn downward. Above the ML the air becomes more stable with altitude and on average this reflects as a transition from a uniform ML potential temperature ($\frac{\partial\overline{\theta}}{\partial z} \approx 0$) to a stable lapse rate (γ). A peak in the average vertical gradient ($\frac{\partial\overline{\theta}}{\partial z}$) at the inversion represents regions where thermals have exceeded their natural buoyancy level.

Nelson et al. in [12] outline the stages of CBL growth from when the sublayers of the nocturnal boundary layer are entrained, untill the previous day's capping inversion is reached and a quasi-steady state growth is attained. The EL depth relative to CBL height varies throughout these stages and its

relationship to scaled entrainment is hysteresial. Numerical studies typically represent this last quasi-steady phase, since there is usually a constant heat flux working against an inversion and or a stable lapse rate. (Schmidt and Schumann [13], Sorbjan [14], Sullivan et al. [19], Federovich et al. [9], Brooks and Fowler [2])

2.2.2 Convective Boundary Layer Height (h)

The ML is fully turbulent with an on average uniform potential temperature (θ). Aerosol and water vapour concentrations decrease dramatically with transition to the stable upper free atmosphere (FA). So any of these characteristics can support a definition of CBL height (h). Nelson et al. define h in terms of the percentage of ML air and identified it by eye from Lidar back-scatter images in [12]. Traumner et al. compared four automated methods applied to Lidar images: a suitable threshold value above which the air is categorized as ML air, the point of minimum (largest negative) vertical gradient, the point of minimum vertical gradient based on a fitted idealized curve, and the maximum wavelet covariance in [21].

The use of Lidar dominates studies based on measurement. Numerical modelling studies have hundreds of local horizontal points from which smooth averaged vertical profiles be obtained, and statistically robust relationships inferred. Brooks and Fowler [2] applied their wavelet technique to local vertical tracer profiles in their large eddy simulation (LES) study and compared it to the gradient method (i.e. locating the point of minimum vertical gradient) and the point of minimum ($\overline{w'\theta'}$). This last definition has been common in LES and laboratory studies where it's been referred to as the inversion height (Deardorff et al. [7], Sorbjan [15], Federovich et al. [9]). Sullivan et al. [19] clarified that this point does not correspond to the average point of maximum $\frac{\partial\overline{\theta}}{\partial z}$, whereas the upper extrema of the four $\overline{w'\theta'}$ quadrants: upward moving warm air ($\overline{w'^{+}\theta'^{+}}$), downward moving warm air ($\overline{w'^{-}\theta'^{+}}$), upward moving cool air ($\overline{w'^{+}\theta'^{-}}$), downward moving cool air ($\overline{w'^{-}\theta'^{-}}$) more or less did. They defined CBL height based on local $\frac{\partial\theta}{\partial z}$ and applied hori-

zontal averaging as well as two methods based on $\overline{w'\theta'}$ for comparison.

None of the published LES studies so far define the height in terms of the $\overline{\theta}$ or $\frac{\partial\overline{\theta}}{\partial z}$ profile even though bulk models, from which CBL growth parametrizations stem, rely on an idealized version thereof. Garcia and Mellado do include it as one of their measures of CBL height in their direct numerical simulation study (DNS) [11].

2.2.3 Convective Boundary Layer Growth by Entrainment

In the quasi-steady regime the CBL grows by trapping pockets of warm stable air between or adjacent to impinging thermal plumes. Traumner et al. [21] summarize two relevant buoyancy driven regimes of entrainment:

- Non turbulent fluid can be engulfed between or in the overturning of thermal plumes. This kind of event was seen by Sullivan et al. in [19] when the inversion was weak. Traumner et al.'s observations in [21] support this.
- Impinging thermal plumes distort the inversion interface dragging wisps of warm stable air down at their edges or during recoil under a strong inversion or lapse rate. This type of event is supported by the findings of both Sullivan et al. [19] and Traumner et al. [21].

Under atmospheric conditions shear induced instabilities do occur, and in some laboratory studies under conditions of very high stability the breaking of internal waves have been observed. Both processes are believed to result in some entrainment but we do not consider them here since the former is relatively insignificant in strong convection and the latter has not so far been observed in measurements or modeled output of the atmospheric CBL. (Traumner et al. [21], Sullivan et al. [19])

2.2.4 The Convective Boundary Layer Entrainment Layer

The ML is fully turbulent but the top is characterised by stable air with intermittent turbulence due to the higher reaching thermal plumes. Garcia and Mellado demonstrate that the entrainment layer (EL) is subdivided in terms of length and buoyancy scales. That is, the lower region is comprised of mostly turbulent air with pockets of stable warmer air that are quickly mixed, and so scales with the convective scales (see section 2.4). Whereas the upper region is mostly stable apart from the impinging thermal plumes so scaling here is more influenced by the lapse rate (γ).

In the EL the average vertical heat flux ($\overline{w'\theta'}$) switches sign relative to that in the ML. The fast updraughts are now relatively cool ($\overline{w'^{+}\theta'^{-}}$). In their analysis of the four $\overline{w'\theta'}$ quadrants Sullivan et al. [19] concluded that the overall dynamic in this region is downward motion of warm air from the free atmosphere (FA) ($\overline{w'^{-}\theta'^{+}}$) since the other three quadrants effectively cancel.

In terms of tracer concentration and for example based on a Lidar backscatter profile, there are two ways to conceptually define the entrainment layer (EL). It can be thought of as the range in space (or time) over which local height varies (Crum et al. [3]). There is also a local region over which the concentration (or back-scatter intensity) transitions from ML to free atmospheric (FA) values (Traumner et al. [21]). The latter can be estimated using both curve-fitting and wavelet techniques (Traumner et al. [21], Steyn et al. [16], Brooks and Fowler [2]). Traumner et al. [21] compared the two concepts, found them to differ and seem to favour the latter based on how correlated the corresponding scaling relationships were.

Brooks and Fowler apply a wavelet technique to tracer profiles for the determination of EL limits, in their LES study ([2]). But it is more common in numerical modelling and laboratory studies for the EL limits to be defined based on the average vertical heat flux ($\overline{w'\theta'}$) i.e. the point at which it goes from positive to negative values, and the point at which it goes from

negative value to zero (Deardorff et al. [7], Federovich et al. [9], Garcia and Mellado [11]). Bulk first order models assume the region of negative $\overline{w'\theta'}$ coincides with the region where $\overline{\theta}$ transitions from the ML value to the FA value. (Deardorff [6], [9] [9]). But no modelling studies use the vertical $\overline{\theta}$ profile to define the entrainment layer (EL).

Since the mixed layer $\overline{\theta}$ from a numerical model is not strictly constant (Federovich et al. [9]), a threshold value for $\overline{\theta}$ or its vertical gradient must be chosen to identify the lower EL limit. Brooks and Fowler encountered inconsistencies when determining the EL limits from the average tracer profile [2]. But the their tracer profile was different to a simulated $\overline{\theta}$ profile whose ML value increases in time predictably based on the $\overline{w'\theta'}$ from the surface and the CBL top or inversion.

2.3 Modelling the Convective Boundary Layer and Entrainment Layer

2.3.1 Bulk Analytical Models

Bulk analytical models for the Convective Boundary layer (CBL) can be subdivided into: (i) zero order and (ii) first order bulk models.

Zero order bulk models assume a Mixed Layer (ML) of uniform potential temperature ($\overline{\theta}_{ML}$) topped by an infinitesimally thin layer across which there is a temperature jump ($\Delta\theta$) and above which is a constant lapse rate (γ). The assumed vertical heat flux ($\overline{w'\theta'}$) profile is linearly decreasing from the surface up, reaching a maximum negative $\overline{w'\theta'}_h$ value which is a constant proportion of the surface value (usually -.2) at the temperature inversion, and decreasing to zero ac-cross the jump. Equations for the evolution of CBL height, $\overline{\theta}_{ML}$ and $\Delta\theta$ are derived on this basis.

For example, if the CBL height (h) is rising, air is being drawn in from the stable layer above and decreasing in enthalpy. So, the decrease in enthalpy

is $c_p \rho \Delta\theta \frac{dh}{dt}$ per unit of horizontal area. Since above the inversion is stable Tennekes in [20] equates this enthalpy loss to the average vertical flux at the inversion.

$$\Delta\theta \frac{dh}{dt} = -\overline{w'\theta'}_h \tag{2.3}$$

The ML warming rate is arrived at via the simplified reynolds averaged conservation of enthalpy

$$\frac{\partial \overline{\theta}_{ML}}{\partial t} = -\frac{\partial}{\partial z} \overline{w'\theta'} \tag{2.4}$$

which based on the assumed constant slope of the vertical heat flux becomes

$$\frac{\partial \overline{\theta}_{ML}}{\partial t} = \frac{\overline{w'\theta'}_s - \overline{w'\theta'}_h}{h} \tag{2.5}$$

and the evolution of the temperature jump ($\Delta\theta$) depends on the rate of CBL height (h) increase, the upper lapse rate γ and the ML warming rate

$$\frac{d\Delta\theta}{dt} = \gamma \frac{dh}{dt} - \frac{d\overline{\theta}_{ML}}{dt} \tag{2.6}$$

An assumption about the vertical heat flux at the inversion (h), such as the entrainment ratio, closes this set.

$$\frac{\overline{w'\theta'}_h}{\overline{w'\theta'}_s} = -.2 \tag{2.7}$$

(Tennekes [20])

The relevant quantities are idealized ensemble averages. There is some variation within this class of model, for example the rate equation for h (entrainment relation) can alternatively be derived based on the turbulent kinetic energy budget (Federovich et al. [9]). But they are all based on the simplified $\overline{\theta}$ and $\overline{w'\theta'}$ profiles outlined above.

First order models assume an entrainment layer (EL) of finite depth at the top of the ML, defined by two heights: the top of the ML (h_0) and the point

where free atmospheric characteristics are resumed (h_1). The derivations are more complex and examples of simplifying assumptions about the EL are:

- $\Delta h = h_1 - h_0 = Constant$
- Δh or maximum overshoot distance $d \propto \frac{w^*}{N}$ where w^* is the relevant vertical velocity scale and $N = \sqrt{\frac{g}{\overline{\theta}} \frac{\partial \overline{\theta}}{\partial z}}$ is the Brunt-Vaisalla frequency
- and that between h_0 and h_1 $\overline{\theta} = \overline{\theta}_{ML} + f(z,t)\Delta\theta$ where $f(z,t)$ is a dimensionless shape factor

(Deardorff [6], Stull [17]).

Although development of these models is beyond the scope of this thesis, mention of them is necessary to give context to the scaling relationships or parametrizations considered.

2.3.2 Numerical Simulations

Numerical simulation of the convective boundary layer (CBL) is carried out by solving the Navier Stokes equations, simplified according to a suitable approximation, on a discrete grid. Types of simulations can be grouped according to the scales of motion they resolve. In direct numerical simulations (DNS) the full range of spatial and temporal turbulence are resolved from the size of the domain down to the smallest dissipative scales i.e. the Kolmagorov micro-scales. This requires a dense numerical grid and so can be computationally prohibitive. In a large eddy simulation (LES) smaller scales are filtered out and parametrized by sub grid scale closure model. General circulation models (GCM) solve the Navier Stokes equations on a spherical grid and parametrize smaller scale processes including convection and cloud cover.

LES has steadily, repeatedly been used to better understand the CBL since Deardorff applied this relatively new method in [5] for this purpose. Sullivan

et al. in [19], Federovich et al. in [9] and Brooks and Fowler in [2] used it to observe the structure and scaling behaviour of the EL.

2.4 Scales of the CBL and Entrainment Layer

2.4.1 Length Scale (h)

Deardorff in [5] demonstrated that the inversion base height scales the sizes of the dominant turbulent structures in penetrative convection. This was taken to be the height of minimum average vertical heat flux (z_f) (Deardorff et al. [7]). Since then, the concept of CBL height (h) has remained reasonably consistent in that it is measured at the inversion or point, above the surface layer, of maximum change in tracer concentration or potential temperature (θ). Turbulence based concepts, such as the velocity variance and the distance over which velocity is correlated with itself, are related but represent the current turbulent dynamics rather than the turbulence history (Traumner et al. [21]).

2.4.2 Convective Velocity Scale (w^*)

Given an average surface vertical heat flux ($\overline{w'\theta'}_s$) a surface buoyancy flux can be defined as $\frac{g}{\overline{\theta}}\overline{w'\theta'}$ from which the convective velocity scale is obtained by multiplying by the appropriate length scale. Since the result is in $\frac{m^3}{s^3}$ a cube root is applied.

$$w^* = \left(\frac{gh}{\overline{\theta}}\overline{w'\theta'}\right)^{\frac{1}{3}} \tag{2.8}$$

Deardorff ([4]) confirmed that this effectively scaled the vertical turbulent velocity perturbations ($w^{'}$) in the CBL. Sorbjan's work in [14] supports

this, even at the CBL top. $\frac{dh}{dt}$ and $w^{'}$ are driven by $\overline{w^{'}\theta^{'}}_s$ and inhibited by γ. The influence of γ on $w^{'}$ is indirectly accounted for via h in w^*.

2.4.3 Convective Time Scale (τ)

It logically follows that the time for a thermal to reach the top of the CBL is

$$\tau = \frac{h}{\left(\frac{gh}{\overline{\theta}}\overline{w^{'}\theta^{'}}\right)^{\frac{1}{3}}} \tag{2.9}$$

Sullivan et al. showed a linear relationship between h and time scaled by this time scale in [19]. The time scale associated with the buoyant thermals overshooting and sinking (Brunt-Vaisala frequency) is another obvious choice (Federovich et al. [9]). The ratio of these two time-scales forms a parameter which characterizes this system. (see Sorbjan[14] and Deardorff [6])

2.4.4 Convective Temperature Scale (θ^*)

The CBL temperature fluctuations $\theta^{'}$ are influenced by $\overline{w^{'}\theta^{'}}$ from both the surface and the CBL top. Deardorff ([4]) showed that an effective scale based on the convective velocity scale is

$$\theta^* = \frac{\overline{w^{'}\theta^{'}}}{w^*} \tag{2.10}$$

Whereas Sorbjan ([14]) showed that as with proximity to the CBL top the effects of γ become more important.

2.4.5 Buoyancy Richardson Number (Ri)

The flux Richardson (R_f) number expresses the balance between turbulent mechanical energy and buoyancy. It's obtained from the ratio of these two terms in the turbulent kinetic energy budget equation (Stull [18]):

$$\frac{\partial \overline{e}}{\partial t} + \overline{U}_j \frac{\partial \overline{e}}{\partial x_j} = \delta_{i3} \frac{g}{\overline{\theta}} \left(\overline{u_i' \theta'} \right) - \overline{u_i' u_j'} \frac{\partial \overline{U}_i}{\partial x_j} - \frac{\partial \left(u_j' e' \right)}{\partial x_j} - \frac{1}{\overline{\rho}} \frac{\partial \left(u_i' p' \right)}{\partial x_i} - \epsilon \quad (2.11)$$

$$R_f = \frac{\frac{g}{\overline{\theta}} \left(\overline{w' \theta'} \right)}{\overline{u_i' u_j'} \frac{\partial \overline{U}_i}{\partial x_j}} \quad (2.12)$$

Assuming horizontal homogeneity and neglecting subsidence

$$R_f = \frac{\frac{g}{\overline{\theta}} \left(\overline{w' \theta'} \right)}{\overline{u' w'} \frac{\partial \overline{U}}{\partial z} + \overline{v' w'} \frac{\partial \overline{V}}{\partial z}} \quad (2.13)$$

Applying first order closer to the flux terms, i.e. assuming they are proportional to the vertical gradients, gives the gradient Richardson number (R_g)

$$R_g = \frac{\frac{g}{\overline{\theta}} \frac{\partial \overline{\theta}}{\partial z}}{\left(\frac{\partial \overline{U}}{\partial z} \right)^2 + \left(\frac{\partial \overline{V}}{\partial z} \right)^2} \quad (2.14)$$

which expresses the balance between shear and buoyancy driven turbulence, but in the EL buoyancy acts to suppress buoyancy driven turbulence. Applying a bulk approximation to the denominator, and expressing it in terms of scales yields a ratio of two square of time scales

$$R_g = \frac{\frac{g}{\overline{\theta}} \frac{\partial \overline{\theta}}{\partial z}}{\frac{U^{*2}}{L^2}} = N^2 \frac{L^2}{U^{*2}} \quad (2.15)$$

and applying the bulk approximation to both the numerator and the denominator yields

$$R_b = \frac{\frac{g}{\overline{\theta}} \Delta \theta L}{U^{*2}} \quad (2.16)$$

A natural choice of length and velocity scales for the CBL are h and w^*. Ellison and Turner ([8]) suggested and confirmed a relationship between the entrainment rate and this form of Richardson number (Ri) based on tank

experiments. This parameter can be justified and arrived at by considering the principal forcings of the system, or from non-dimensionalizing the entrainment relation derived analytically (Tennekes [20], Deardorff [5]).

$$w_e \propto \frac{\overline{w'\theta'}_s}{\Delta\theta} \tag{2.17}$$

$$\frac{w_e}{w^*} \propto \frac{\overline{w'\theta'}_s}{\Delta\theta w^*} = Ri^{-1} \tag{2.18}$$

In one or other of its forms this parameter has become central to any study on CBL entrainment (Sullivan et al. [19], Federovich et al. [9], Traumner et al. [21], Brooks and Fowler [2])

2.4.6 Relationship of Entrainment Rate and Entrainment Layer Depth to Richardson Number

The relationship between scaled entrainment rate and the buoyancy Richardson number (Ri) is arrived at according the zero order bulk model through thermodynamic arguments, or by integration of the conservation of enthalpy or turbulent kinetic energy equations over the growing CBL. (Tennekes [20], Deardorff [6], Federovich et al. [9]).

$$\frac{w_e}{w^*} \propto Ri^{-a} \tag{2.19}$$

It has been verified in numerous laboratory and numerical studies (Deardorff et al. [7], Sullivan et al. [19], Federovich et al. [9], Brooks and Fowler [2]). But there is still some unresolved discussion as the the exact value of a. It seems there are two possible values, $-\frac{3}{2}$ and -1, the first of which Ellison and Turner ([8]) suggested occurs at high stability when buoyant recoil of impinging thermals becomes more important than their convective overturning. Federovich et al. ([9]) arrive at this power law through an Ri obtained using the potential temperature jump across the EL.

A relationship of the scaled entrainment layer EL depth to Ri is arrived at by considering the deceleration of a thermal as it overshoots its natural

buoyancy level (Nelson et al. [12]), such that its overshoot distance is

$$d \propto \frac{w^{*2}}{\frac{g}{\bar{\theta}_{ML}}\Delta\theta} \tag{2.20}$$

If the EL depth is proportional to the overshoot distance then

$$\frac{\Delta h}{h} \propto \frac{w^{*2}}{\frac{g}{\bar{\theta}_{ML}}h\Delta\theta} = Ri^{-1} \tag{2.21}$$

Boers [1] integrated the potential and thermal energy difference before and after distortion of the inversion interface with the assumption that the resulting variation in the shape is sinusoidal. He equated this to the total kinetic energy of the CBL and arrived at a $-\frac{1}{2}$ power law relationship

$$\frac{\Delta h}{h} \propto Ri^{-\frac{1}{2}} \tag{2.22}$$

2.5 Approach to Research Questions

Similar to (list) I will model the dry shear free convective boundary layer using Large Eddie Simulation, specifically the cloud resolving model of Marat System for Atmospheric Modelling (SAM). The set up will be slightly different in that I will use a slightly smaller domain than usuall (vs 5x5) but I will run a 10 case ensemble to obtain true ensemble averages and so turbulent potential temperature perturbations. The chosen grid sizes were very much influenced by the **?** **?** and in the vertical is of higher resolution than the other comparable studies (Sull Moeng, Fed, BandF). Before addressing the questions stated in Section 2.1 I'll examine the model to make sure it represents a realistic turbulent CBL in Section **??**. I will look at the averaged vertical profiles of velocity and temperature, and tunrbulet kinetic energy as represented my the root mean squared velocity profiles and make sure they are in line with those seen before (SchmidtSchu, Sull, Fed). I will look at the local temperature and velocity profiles to see that coherent thermals are being produced. I will look at the fft energy density spectra to see that there is adequate scale separation between the most energy intense structures and

the grid spacing and that there is a slope corresponding kolmagorov power law. I will initiallize with a constant surface heat flux acting a against a uniform lapse rate. This is different to Sullivan and Moeng and Brooks and Fowler. They obtained a range of Ri by varying an imposed a θ jump while keeping the same γ. So here, the θ jump arises from the overshoot of the thermals (references here, Garcia Mellado).

2.5.1 Q1: How do the distrubutions of local CBL height, and $\theta^{'}w^{'}$ within the EL, vary with $\overline{w^{'}\theta^{'}}_{s}$ and γ?

The EL can be thought of in terms of the distribution of the thermal heights, or local heights. Sullivan and moeng measured local height by locating the vertical point of maximum gradient, and observed the effects of varying Ri on the resulting distributions. However this method is problematic when gradients in the upper profile exceed that at the inversion (cite BandF). Steyn et al fitted an idealized curve to a lidar backscatter profile. This method produces a smooth curve ased on the full original profile on which a mximum can easily be located. Similarly, I will apply a multi-linear regression method outlined in **?** to the local θ profiles one line representing the ML, EL and FA and locate the ML top. I'll observe how the resulting distributions are effected by changes in Ri using histograms and verify that the resulting surface corresponds to the location of the termals in the EL (See Section)

Sullivan and Moeng broke the turbulent vertical heat flux into four quadrants and used this combined with local flow visualizations to show how the thermals impinge and draw down warm air from above. Mahrt and Paulmier used 2 dimensional contour plots of local $w^{'}$ and $\theta^{'}$ on measurements and analysed their joint distribubions. In his LES study Sorbjan showed that in the CBL in particular in the EL $\theta^{'}$ is strongly influenced by γ whereas $w^{'}$ is independent thereof. Influenced by these three studies, I will use 2 dimensional histograms at three levels within the EL to look at how the distrubutions of local $w^{'}$ and $\theta^{'}$ are effected by changes in γ and $\overline{w^{'}\theta^{'}}_{s}$. I will try to isolate the effects of γ, other than on the heights reached, by

applying the convective scales, θ^* and w^*.

2.5.2 Q2: How can the EL limits be defined based on the $\overline{\theta}$ profile and what is the relationship of the resulting depth (Δh) to Ri?

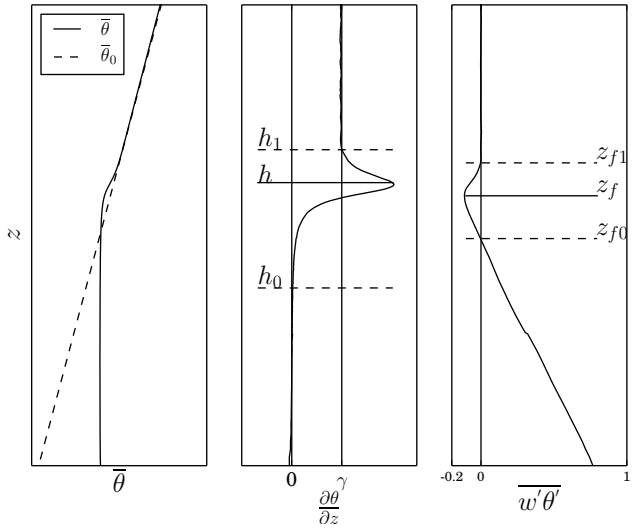

Figure 2.3: Height Definitions Based on the Average Vertical Profiles

CBL Height	ML $\overline{\theta}$	EL Limits	θ Jump		Ri
h (see Figure 2.3)	$\overline{\theta}_{ML} = \frac{1}{h}\int_0^h \overline{\theta}(z)dz$	h_0, h_1	$\delta\theta$ $\overline{\theta}(h_1)$ $\overline{\theta}(h_0)$	$= -$	Ri $= \frac{\delta\theta}{\frac{\overline{w'\theta'}_s}{w^*}}$
			$\Delta\theta$ $\overline{\theta}_0(h) - \overline{\theta}_{ML}$	$=$	Ri$= \frac{\Delta\theta}{\frac{\overline{w'\theta'}_s}{w^*}}$

Table 2.1: Relevant Definitions used in this Study

2.5.3 Q3: How does defining the θ jump based on the vertical $\overline{\theta}$, i.e. accross the EL as in Figure 2.1 vs at the inversion (h) as in Figure 2.2, effect the entrainment relation, in particular a?

Bibliography

[1] R. Boers. A parametrization of the depth of the entrainment zone. *Journal of Applied Meteorology*, pages 107–111, 1989. → pages 4, 17

[2] I. M. Brooks and A. M. Fowler. An evaluation of boundary-layer depth, inversion and entrainment parameters by large-eddy simulation. *Bundary-Layer Meteorology*, 142:245–263, 2012. → pages 2, 4, 7, 9, 10, 13, 16

[3] T. D. Crum, R. B. Stull, and E. W. Eloranta. Coincident lidar and aircraft observations of entrainment into thermals and mixed layers. *Journal of Climate and Applied Meteorology*, 26:774–788, 1987. → pages 5, 6, 9

[4] J. W. Deardorff. Convective velocity and temperature scales for the unstable planetary boundary layer and for rayleigh convection. *Journal of the Atmospheric Sciences*, 27:1211 – 1213, 1970. → pages 2, 13, 14

[5] J. W. Deardorff. Numerical investigation of neutral and unstable planetary boundary layers. *Journal of the Atmospheric Sciences*, 29: 91 – 115, 1972. → pages 12, 13, 16

[6] J. W. Deardorff. Prediction of convective mixed-layer entrainment for realistic capping inversion structure. *Journal of the Atmospheric Sciences*, 36:424–436, 1979. → pages 4, 10, 12, 14, 16

[7] J. W. Deardorff, G. E. Willis, and B. J. Stockton. Laboratory studies of the entrainment zone of a convectively mixed layer. *J. Fluid Mech.*, 100:41–64, 1980. → pages 2, 4, 7, 10, 13, 16

[8] T. H. Ellison and J. S. Turner. Turbulent entrainment in stratified flows. *Journal of Fluid Mechanics*, 6:423–448, 1959. → pages 15, 16

[9] E. Federovich, R. Conzemus, and D. Mironov. Convective entrainmnent into a shear-free, linearly stratifies atmosphere: Bulk models reevaluated through large eddie simulation. *Journal of the Atmospheric Sciences*, 61:281 – 295, 2004. → pages 2, 4, 5, 7, 10, 11, 13, 14, 16

[10] E. Fedorovich and R. Conzemius. *Large Eddy Simulation of Convective Entrainment in Linearly and Discretely Stratified Fluids*. Kluwer Academic Publishers, 1 edition, 2001. → pages 5

[11] J. R. Garcia and J. P. Mellado. The two-layer structure of the entrainment zone in the convective boundary layer. *Journal of the Atmospheric Sciences*, 2014. doi:10.1175/JAS-D-130148.1. → pages 2, 5, 8, 9, 10

[12] E. Nelson, R. Stull, and E. Eloranta. A prognostic relationship for entrainment zone thickness. *Journal of Applied Meteorology*, 28: 885–901, 1989. → pages 2, 4, 6, 7, 17

[13] H. Schmidt and U. Schumann. Coherent structure of the convective boundary layer derived from larg-eddy simulations. *J. Fluid. Mech.*, 200:511–562, 1989. → pages 6, 7

[14] Z. Sorbjan. Effects caused by varying the strenth of the capping inversion based on a large eddie simulation of the shear free convective boundary layer. *Journal of the Atmospheric Sciences*, 53:2015 – 2023, 1996. → pages 2, 3, 7, 13, 14

[15] Z. Sorbjan. Similarity of scalar fields in the convective boundary layer. *Journal of the Atmospheric Sciences*, 56:2212 – 2221, 1999. → pages 7

[16] D. G. Steyn, M. Baldi, and R. M. Hoff. The detection of mixed layer depth and entrainment zone thickness from lidar backscatter profiles. *Journal of Atmospheric and Oceanic Technology*, 16:953–959, 1999. → pages 2, 9

[17] R. Stull. Inversion rise model based on penetrative convection. *Journal of the Atmospheric Sciences*, 30:1092–1099, 1973. → pages 12

[18] R. Stull. *An Introduction to Boundary Layer Meteorology*. Kluwer Academic Publishers, 1 edition, 1988. ISBN 9027727686. → pages 1, 2, 5, 14

[] P. P. Sullivan and E. G. Patton. The effect of mesh resolution on convective boundary layer statistics and structures generated by large eddie simulation. *Journal of the Atmospheric Sciences*, 58:2395–2415, 2011. doi:10.1175/JAS-D-10-05010.1. → pages

[19] P. P. Sullivan, C.-H. Moeng, B. Stevens, D. H. Lenschow, and S. D. Mayor. Structure of the entrainment zone capping the convective atmospheric boundary layer. *Journal of the Atmospheric Sciences*, 55: 3042–3063, 1998. doi:10.1007/s10546-011-9668-3. → pages 2, 5, 6, 7, 8, 9, 12, 13, 14, 16

[20] H. Tennekes. A model for the dynamics of the inversion above a convective boundary layer. *Journal of the Atmospheric Sciences*, 30: 558–566, 1973. → pages 4, 11, 16

[21] K. Traumner, C. Kottmeier, U. Corsmeier, and A. Wieser. Convective boundary-layer entrainment: Short review and progress using doppler lidar. *Bundary-Layer Meteorology*, 141:369–391, 2011. doi:10.1007/s10546-011-9657-6. → pages 2, 5, 6, 7, 8, 9, 13, 16

[22] J. S. Turner. Turbulent entrainment: the development of the entrainment assumption and its application to geophysical flows. *J. Fluid Mech.*, 173:431–471, 1986. → pages 5

[] E. Vieth. Fitting piecewise linear regression functions to biological responses. *Journal of Applied Physiology*, 67:390–396, 2011. → pages